ADVANCED MATERIALS INTERFACES
Open Access
www.advmatinterfaces.de

Tailoring of Creep Regime Domain Wall Dynamics in Perpendicularly Magnetized Pd/Co/Pd Trilayers

*Anurag Keloth, Rakhul Raj, V. Raghavendra Reddy, Mukul Gupta, Ilaria Carlomagno, Andrei Gloskovksii, Timo Kuschel, Ajay Gupta, and Sarathlal Koyiloth Vayalil**

Understanding magnetic domain wall (DW) dynamics is vital for improving the performance of heavy metal/ferromagnet based spintronic devices. Pd/Co/Pd multilayers hosting perpendicular magnetic anisotropy and interfacial Dzyaloshinskii-Moriya interaction are prototypes for high density magnetic memory devices. This work presents the creep regime DW dynamics in Pd/Co/Pd trilayers with Ta buffer layer excited by symmetric field-induced domain wall motion using Kerr microscopy. A systematic increment of DW velocity with increasing Co thickness is observed. SQUID-VSM measurements reveal that the effective anisotropy constant decreases with the Co layer, leading to an increased DW width. Kerr microscopy images confirm that the DW is becoming rougher with magnetic layer thickness because of the dominance of magnetostatic energy over the DW energy. Hard X-ray photoemission spectroscopy (HAXPES) reveals the presence of alloying at interfaces of Co/Pd. The asymmetry in magnetic circular dichroism HAXPES at the Pd 3d edge pictures the induced magnetic moment in Pd which is consistent with the larger saturation magnetization obtained from vibrating sample magnetometry. Extended X-ray absorption fine structure performed in out-of-plane and in-plane geometry shows the disordered nature of the Co local environment with the interdiffusion of Pd atoms into Co causing an asymmetry in the bonds.

1. Introduction

In recent years, heterostructures with heavy metal (HM)/ferromagnet (FM) multilayers gained attraction in spintronics based memory-logic devices owing to their vast applications.[1–4] In this kind of multilayer systems, the HM/FM interfaces are the region of origin of major phenomena such as perpendicular magnetic anisotropy (PMA),[5] spin-orbit torque (SOT),[6] spin Hall effect (SHE),[7] interfacial Dzyaloshinskii-Moriya interaction (iDMI)[8,9] etc. Typical HM/FM/HM structures viz. Pt/Co/Pt, Pd/Co/Pd, Pt/CoFeB/Pt multilayers, in which an ultra-thin FM film is interfaced with HM layers, are very widely investigated for PMA, iDMI, SOT.[6,10,11] DMI stabilizes chiral spin textures[12] and skyrmions[13] which are promising candidates for spintronics based memory and logic devices. PMA is a very fascinating phenomenon in spintronic-based devices for high-density data storage, offering a significant energy barrier against thermal fluctuations without causing harm to data reliability. It has been observed that SOT-based memory devices exhibit a high critical current density for magnetization reversal.[14,15] However, to achieve lower power consumption, a reduced critical switching current density is recommended. The interface engineering in heterostructures is an efficient method to control the SOT efficiency and the switching current density. Interfacial

A. Keloth, A. Gupta, S. Koyiloth Vayalil
Department of Physics
Applied Science Cluster
UPES
Dehradun 248007, India
E-mail: sarathlal.koyiloth.vayalil@desy.de

R. Raj, V. R. Reddy, M. Gupta
UGC-DAE Consortium for Scientific Research
University Campus, Khandwa Road, Indore 452001, India

I. Carlomagno
Elettra Sincrotrone Trieste
Strada Statale 14, km 163.5 in AREA Science Park, Basovizza, Trieste 34149, Italy

A. Gloskovksii, S. Koyiloth Vayalil
Deutsches Elektronen-Synchrotron DESY
Notkestraße 85, 22607 Hamburg, Germany

T. Kuschel
Center for Spinelectronic Materials and Devices
Department of Physics
Bielefeld University
Universitätsstraße 25, 33615 Bielefeld, Germany

The ORCID identification number(s) for the author(s) of this article can be found under https://doi.org/10.1002/admi.202400804

DOI: 10.1002/admi.202400804

interdiffusion can enhance PMA and SOT while reducing the critical current density for magnetization reversal in the Ta/Pt/Co/Ta system with an improved spin Hall angle (SHA).[16]

In the above-mentioned kind of multilayers, different interfaces play a major role in domain dynamics. In Co/Pt systems, the signs of DMI and SHE-STT (spin-transfer torque) are different across top and bottom interfaces[17] and the strength of DMI in the Co layer close to interface are very strong compared to the other layers.[18] Further, Pd/Co/Pd trilayers with DMI were identified to be host for zero field, room temperature skyrmions.[3,4]

Comprehending the dynamics of domain walls (DW), which are the boundaries that separate regions with different magnetization, is essential for enhancing device performance. As far as the spintronic-based data storage devices, such as race track memories, where the data is stored in the magnetic domains and transmitted through DW motion along a track, thus DW motion is crucial. These DWs could interfere with the defects in the system, which alters its response and results in the pinning. DWs are too thin in the magnitude of nanometers in multilayer systems with PMA like Pd/Co/Pd, Pt/Co/Pt, etc. and they are heavily subjected to the pinning by the atomic imperfections in the system. Thus, from a technological point of view, the study of DW in these kinds of systems is of great interest because it is easy to control it using external factors like magnetic field and current, making it suitable for DW race tracks and memory logic devices. The DW dynamics is classified into various regions such as creep, depinning and flow regimes. In the creep regimes, the thermal fluctuation favors the DW motion overtaking high pinning and local equilibrium of DW's. The field-induced domain wall motion (FIDWM)[19] or the use of charge current[6] combined with Kerr microscopy are most commonly used techniques to study the DW motion. The magneto-optical Kerr effect (MOKE) serves as a non-destructive simple technique to study various phenomena in magnetic based system viz. magnetic anisotropy,[20] iDMI[21] etc.

Structural and interfacial properties of thin films can be tuned to engineer the magnetic properties of HM/FM devices. The interfacial phenomena such as interdiffusion, alloying etc. influence the magnetization dynamics of the system. It is reported that the magnetization dynamics of induced moments in Pt sub-lattice is entirely different compared to that of Co sublattice moments in Co-Pt systems.[22] Interfacial effects such as the magnetic proximity effect (MPE), for which a few monolayers of the HM in close vicinity to the FM get magnetized, which is also reported to be asymmetric across different HM/FM interfaces,[23–25] may alter the iDMI in HM/FM multilayers.[25] Vineeth et al. showed that the domain structure in Pt/Co/Pt trilayers can be tuned by Cu dusting on top as well as bottom interfaces and lead to the variation of the PMA.[26] The optimization and design of DW-based devices, which requires high DW speed, need the proper understanding of DW dynamics in the low magnetic field region. The thickness and interfacial roughness of the FM layer are crucial parameters when determining the magnetic properties such as PMA, iDMI etc. Jaehun Cho et al. showed the inverse relation of DMI strength and FM layer thickness using Brillouin light scattering spectroscopy on Pt/Co/AlO_X and Pt/CoFeB/AlO_x.[27] The quality of interfaces marked by the extent of intermixing, interfacial roughness etc. influences the shape of the magnetic domains and the DW velocity.[28]

In multilayer heterostructures, spontaneous intermixing of different layers is initiated during the film deposition itself. The Co/Pd multilayers are well known to exhibit interfacial alloying even at room temperature evidenced by various techniques such as nuclear magnetic resonance (NMR),[29] extended X-ray absorption fine structures (EXAFS)[30] etc in Co/Pd multilayer based systems. The Co atoms at the vicinity of the Pd atoms exhibit a more alloy kind of character than the Co atoms in the bulk which has been studied using polarized EXAFS.[31]

In this paper, a systematic study of magnetization dynamics in Pd/Co/Pd trilayers with Ta buffer layer in the creep regime of DW dynamics is presented. Thickness values of the FM layer plays a very crucial role on the magnetization of the HM/FM/HM based multilayer system. Here we show how this affects the structural properties and DW velocity of the Pd/Co/Pd system. Owing to the presence of strong PMA and DMI in Pd/Co/Pd, this work presents the creep regime DW dynamics in Pd/Co/Pd trilayers as a function of magnetic layer thickness values. Kerr microscopy based on MOKE combined with FIDWM is extensively used for studying the DW dynamics.[19,32] Additionally, the chemical and electronic properties are analyzed using hard X-ray photo emission spectroscopy (HAXPES) and X-ray absorption near edge spectroscopy (XANES). The MPE in Pd is confirmed using magnetic circular dichroism HAXPES (MCD-HAXPES) and X-ray resonant magnetic reflectivity (XRMR) studies.

2. Results and Discussions

Figure 1a shows the schematic of deposited Pd (4 nm)/Co (t_{Co} nm)/Pd (2 nm) trilayers with a Ta (4 nm) buffer layer. XRR plots of all as prepared samples are shown in Figure 1b as a function of the scattering vector $q = \frac{4\pi}{\lambda}\sin(\theta)$ ($\theta$is the incidence angle and λ the wavelength of incident and reflected X-rays). XRR data were fitted to obtain the layer thickness and the interface roughness values (shown in **Table 1**) which shows that the thickness of individual layers in multilayers is close to the nominal thicknesses and are of good quality. The bottom Pd/Co and top Co/Pd interfaces have similar roughness (σ).

To study the interfacial chemical and electronic structure of Pd/Co/Pd trilayers, HAXPES measurements were carried out on samples with different Co layer thickness values (C2, C3 and C4). The Co $2p_{3/2}$ HAXPES spectra collected for sample C3 is presented in **Figure 2a**. The obtained data were fitted with an asymmetric peak corresponding to metallic Co, the main peak of Co° centered at 778.1 eV. An extra peak is present in the higher binding energy region of 779.2 eV, which is well below that of known oxides of Co.[33] In literature, such peak has been attributed to alloy of Co with heavy metals.[34–36] Therefore, in the present case, the peak at 779.2 eV can be assigned to the formation of the alloy with Pd at the top and bottom interfaces. Peaks at 780.6 eV and 782.9 eV are two plasmon loss peaks attributing to surface and bulk plasmons,[37] respectively. One can see that the Co^0 peak intensity increases as the sample goes from sample C2 to C4 (inset of Figure 2a), indicating the increasing contribution of bulk Co with increasing layer thickness values. The details of HAXPES fitting for samples C2 and C4 are presented in supplementary section Figure S1a,b, Supporting Information (Including Refs. [37,38]).

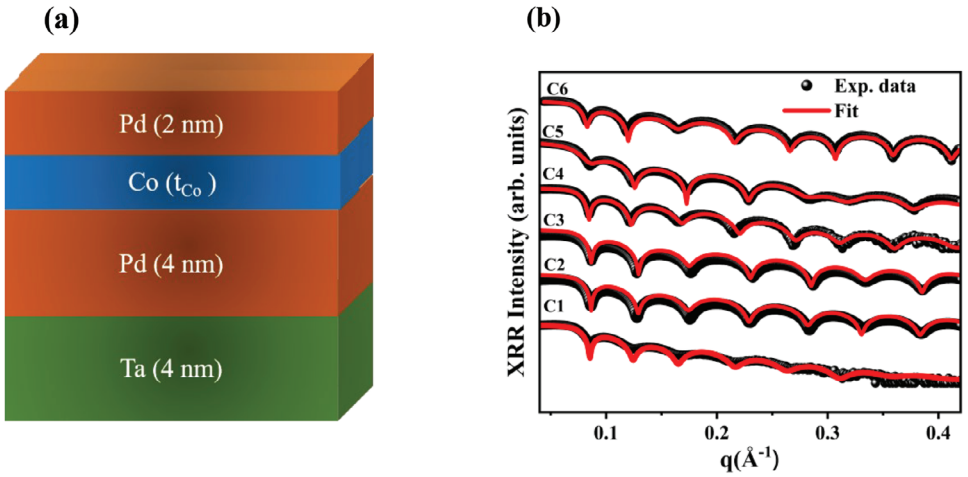

Figure 1. a) Schematic of deposited Ta (4nm)/Pd (4nm)/Co (t_{Co})/Pd (2nm), t_{Co} = 0.3, 0.4, 0.6, 0.8, 0.9, 1.5 nm (C1-C6) b) Fitted XRR data of C1-C6 sample systems plotted with a Y offset for the easiness of viewing.

MCD-HAXPES performed on sample C6 with highest Co layer thickness in the presented series and having in-plane magnetic anisotropy (discussed in the upcoming section) shows a spin-orbit (SO) splitting of Co 2p level into two sub states $2p_{1/2}$ and $2p_{3/2}$ separated by 14.8 eV[39] and shows a clear asymmetry (Figure 2b) as expected. Asymmetry was calculated using the equation $A = \frac{I^+ - I^-}{I^+ + I^-}$; where I^+ and I^- corresponds to the intensity for photon with parallel and anti-parallel helicity and we obtained a maximum MCD asymmetry signal of −14% at the $2p_{3/2}$ main peak line. The satellites peaks observed in the higher binding energy region contributes to the asymmetry after the $2p_{3/2}$ line and a dichroism observed at the tail end after the $2p_{1/2}$ line as shown in the inset of Figure 2b. The considerable MCD asymmetry signal between $2p_{3/2}$ and $2p_{1/2}$ can be attributed to the electron correlation effect due to the configurational mixing caused by the interaction of core-level electrons with valence electrons.[40] Figure 2c represents the MCD-HAXPES spectra corresponding to the Pd-3d edge which also shows a SO splitting into $3d_{5/2}$ and $3d_{3/2}$ states separated by 5.35 eV. A clear dichroism could be observed from the Pd-3d edge MCD-HAXPES (inset of Figure 2c). Since Pd is known to be a Pauli paramagnet having high paramagnetic susceptibility, the observed asymmetry could be attributed to the MPE[23,24] in a few monolayers of Pd induced by the Co layer. The interface sensitive XRMR performed at Pd L_3 edge for sample with in-plane magnetic easy axis drew a clear picture of the MPE in the Pd layer. XRMR data, and asymmetry ratio are shown in supplementary section Figure S2a,b, Supporting Information, respectively (including refs. [41,42]).

XAS spectra collected on sample C3 in two different geometries: with the polarization vector (shown in Figure S3a, Supporting Information) of incident x-rays parallel or perpendicular to the film plane. The smearing of the spectral features, compared to metallic Co, is due to the low thickness of the film and to the high substrate roughness. These, indeed, result into a disordered environment with a large fraction of undercoordinated Co atoms, ending up into smoothened oscillations.[43] The spectra look similar in terms of edge energy and oscillations in the near edge region, showing only a small difference in the very first peak. This difference is similar to the one observed in hcp Co[44] pointing out to a slightly elongated lattice in the direction perpendicular to the film. Around 7800 eV, the signals start to differ from each other. This can be better appreciated looking at the k^2 -weighted EXAFS spectra (**Figure 3a**), where a misalignment in the oscillations becomes evident ≈6 Å^{-1}.

In Figure 3b we show the moduli of the Fourier Transform (FT) of the EXAFS signals, uncorrected for the phase shift. The main peak, ≈2 Å, corresponds to the Co-Co nearest neighbour bond distance, while the second peak, ≈2.6 Å corresponds to the further Co-Pd bond. Both these peaks show a small deviation for the two geometries, with the out-of-plane data showing a slightly

Table 1. Structural parameters, thickness t (± 0.1 nm) and roughness σ (± 0.05 nm) in nm for the sample systems (C1-C6) obtained from the best fit of XRR.

Sample	$\sigma_{Substrate}$ [nm]	t_{Ta} [nm]	σ_{Ta} [nm]	t_{Pd1} [nm]	σ_{Pd1} [nm]	t_{Co} [nm]	σ_{Co} [nm]	t_{Pd2} [nm]	σ_{Pd2} [nm]
C1	0.41	4.6	0.44	4.0	0.45	0.3	0.42	2.5	0.60
C2	0.33	4.6	0.42	4.4	0.37	0.4	0.32	2.1	0.29
C3	0.33	4.5	0.43	4.4	0.34	0.6	0.34	2.3	0.40
C4	0.45	4.6	0.44	4.5	0.40	0.8	0.45	2.2	0.45
C5	0.41	4.4	0.42	4.3	0.36	0.9	0.46	2.1	0.60
C6	0.40	4.5	0.43	4.5	0.33	1.5	0.37	2.0	0.25

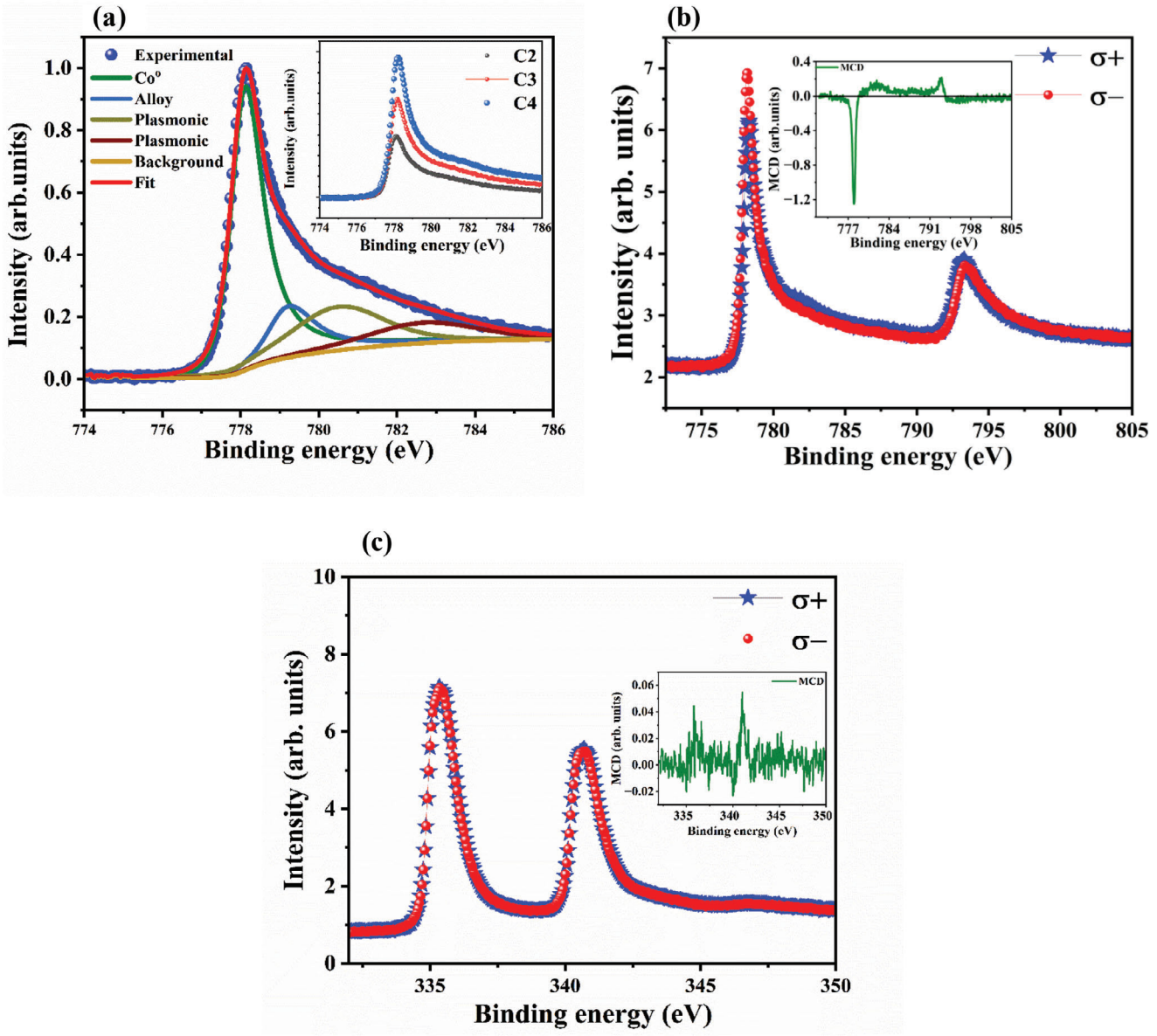

Figure 2. a) HAXPES spectra of sample C3 – Ta(4 nm)/Pd(4 nm)/Co(0.6 nm)/Pd(2 nm) for Co $2p_{3/2}$; inset shows the raw data for the samples C2, C3 and C4 b) MCD-HAXPES obtained for C6 – Ta(4 nm)/Pd(4 nm)/Co(1.5 nm)/Pd(2 nm) at the Co 2p edge; inset shows the MCD c) MCD-HAXPES obtained for C6 – Ta(4 nm)/Pd(4 nm)/Co(1.5 nm)/Pd(2 nm) at the Pd 3d edge; inset shows the MCD.

smaller R value with respect to the in-plane data. This indicates a local anisotropy in the Co-Co and Co-Pd distances, with a small expansion in the direction perpendicular to the film plane and a small contraction along the film plane. This suggests an in-plane compressive stress in the Co film. The peaks above 3 and 3.5 Å, partially unresolved in the out-of-plane data, point out to a higher degree of disorder in the perpendicular direction around Co. Going toward further shells, that is, inspecting the peaks ≈4 and 5 Å, we observe a larger difference in the peaks positions, indicating larger anisotropy. In general, the lower intensity of out-of-plane peaks can be due to the contribution of interface Co atoms being undercoordinated with respect to the central atoms. All these observations are compatible with some Pd gradually entering the Co film structure at the interfaces (i.e., affecting mainly the perpendicular direction), introducing disorder in the structure and stretching the average bond between Co and its neighbors in the out-of-plane direction.

Interfacial alloying as observed from the HAXPES can be correlated to the interdiffusion of Pd atoms into Co layer at interfaces as confirmed by EXAFS which also induces an anisotropy in bond length in perpendicular directions and disorderness. While Carvalho and team reported that an interdiffusion of Pd and Co atoms at interfaces in sputtered Pd/Co/Pd multilayers stabilizes skyrmion phases in the multilayers by enhancing the DMI strength.[45] Also, these kind of interdiffusion of atoms could facilitate the 4d-5d hybridization across the interfaces[46] leading

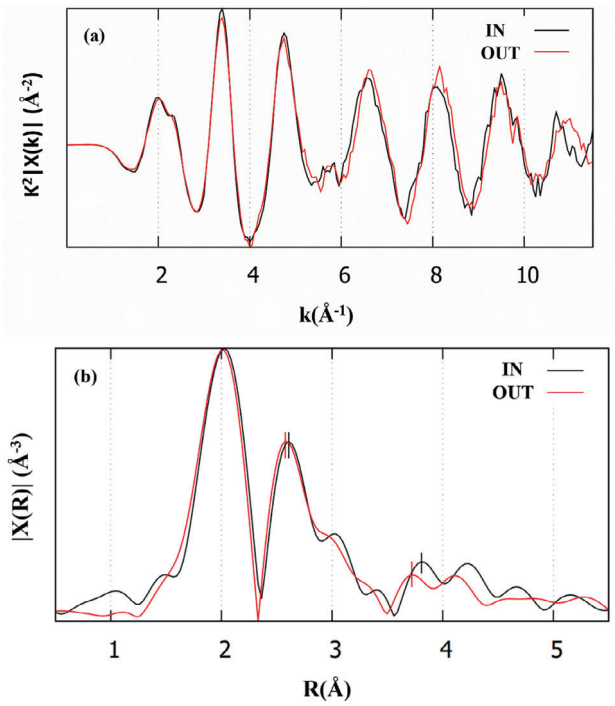

Figure 3. a) k^2 weighted EXAFS spectra for sample C3. b) Fourier transform of EXAFS spectra collected with X-ray polarization vector out plane (red curve) and in plane (black curve) to the sample plane.

to induced magnetic moment (MPE) in Pd at interfaces as confirmed by the asymmetry in XRMR and MCD- HAXPES at Pd absorption edge.

Figure 4a shows PMOKE hysteresis loops measured for C1-C6. Squared hysteresis loops (remanence ratio $\frac{M_R}{M_S} = 1$) confirm the presence of strong PMA in samples C1-C4 which gradually deteriorates with increase of the Co layer thickness. The PMA in the present system can be attributed to the electronic hybridization of Co 3*d* and Pd 4*d* at interfaces.[47] The magnetization reversal in the samples C1-C4 is accompanied by the nucleation of bubble domains owing to high PMA in these systems, whereas no bubbles were observed in the other two samples. Representative bubble domain nucleation and expansion during magnetization reversal in the sample C3 is shown in Figure 4b. Sample C5 (t_{Co} = 0.9 nm) shows weak PMA ($\frac{M_R}{M_S} = 0.2$) and for sample C6 (t_{Co} = 1.5 nm) an applied field of 40 mT is found to be insufficient to saturate the sample in the out-of-plane direction, which is due to the fact that this sample exhibits in-plane magnetic anisotropy, as evidenced from the LMOKE loop (shown in Figure 4c). Furthermore, the coercive field H (c) increases from 15.5 mT for C1 to 26.8 mT for C2. Afterward, the coercivity decreases systematically with increasing Co film thickness and becomes 2.8 mT for C5 with a 0.9 nm Co layer. A similar trend in coercivity with a Co layer thickness was previously observed in trilayer systems.[48–50]

The systematic analysis of PMOKE hysteresis as a function of Co layer thickness values shows a transition from out-of-plane magnetic easy axis (PMA) to out-of-plane hard axis, which happens at a Co film thickness of about $t_{Co} = 0.9$ nm owing to the fact that PMA is an interfacial phenomenon. The LMOKE hysteresis loops of C6 (Figure 4c) measured for 0^0, 45^0 and 90^0 in-plane azimuthal angles are found to be similar in shape, indicating that the sample is magnetically isotropic in the film plane.

To study the DW dynamics, DW velocity measurements were performed on the samples C1, C2, C3 and C4 near the coercive region of each one, where tiny magnetic bubbles start to nucleate and expand throughout the film as the magnetic field increases using symmetric FIDWM by the help of Kerr microscopy.[19] In systems with PMA the DW dynamics can be modeled as the motion of a 1D elastic interface in a 2D disordered medium using a universal creep law.[51] In the low force (low magnetic field) creep regime, the DWs are pinned by multiple defects in the system and the movement is favored by the thermal fluctuations later followed by higher magnetic field depinning and flow regime.[51] The creep scaling law is given by $v = v_0 \exp(\frac{-\alpha}{k_B T} H^{-\frac{1}{4}})$, with $\alpha = U_C \left(\frac{1}{H_{de_P}}\right)^{-\frac{1}{4}}$ being the creep scaling constant, v_0 is the pre-factor, U_C is the parameter that is related to the DW pinning energy barrier, H_{de_P} is the depinning field, H is the magnetic field, k_B is the Boltzmann constant and T is the temperature.

Figure 5a shows the DW velocity plotted against the applied magnetic field H normalized to the coercive field for each sample $(\frac{H}{H_c})$. The linear behavior of $\ln(v)$ v/s $(\frac{H}{H_c})^{-1/4}$ shown in Figure 5b confirms that the DW velocity in the present systems is in accordance with the creep scaling law and that the slope of $\ln(v) - (\frac{H}{H_c})^{-1/4}$ is changing with Co layer thickness. Purple straight line is the creep scale law fit for velocity data. (Representative displacement-pulse width plots for all three samples at an applied magnetic field of 12.6 mT are shown in supplementary section as Figure S4, Supporting Information, from which velocities have been calculated for corresponding magnetic field strengths). The creep parameters α and v_0 are calculated from the slope and intercept of $\ln(v) - (\frac{H}{H_c})^{-1/4}$ It is clear that there is a large variation in the order of magnitude of velocity within a small increment of magnetic field (Figure 5a,b), which can be attributed to DW motion in the thermally activated creep regime. Also, the DWs of sample C4 with t_{Co} = 0.8 nm (sample C4) are found to be almost 1000 times faster than those of thin Co layer films with t_{Co} = 0.3 nm (sample C1) near the coercive region. A systematic increase in the velocity is observed as a function of the value of the Co layer thickness.

The prefactor v_0 can be expanded as[52] $v_0 = d_0 f_0 \exp(\frac{U_c}{k_B T})$, with d_0 being the correlation length of the disorder and f_0 being the attempt frequency. It was observed that f_0 scales with DW mobility and inversely with the Gilbert damping.[52] Also, the Gilbert damping in HM/FM multilayers viz. Pd/Co and Pt/Co decreases with increase of the FM layer thickness.[53,54] The large increase in velocity with the increase in thickness of the Co layer observed in our system could be attributed to the reduction of the damping parameter. The α obtained for sample C4 is $1.84 \times 10^{-19}\ JT^{1/4}$ which drops to $0.94 \times 10^{-19}\ JT^{1/4}$ for sample C1. The variation of α with t_{Co} is shown in Figure 5c. One can easily find that α is linearly varying with t_{Co}. This linear dependence of the creep scaling constant with thickness of the Co layer shows that Pd/Co/Pd trilayers are intact with the creep scaling law in the thermally activated low-field regime of the DW motion.[55,56] Variation of

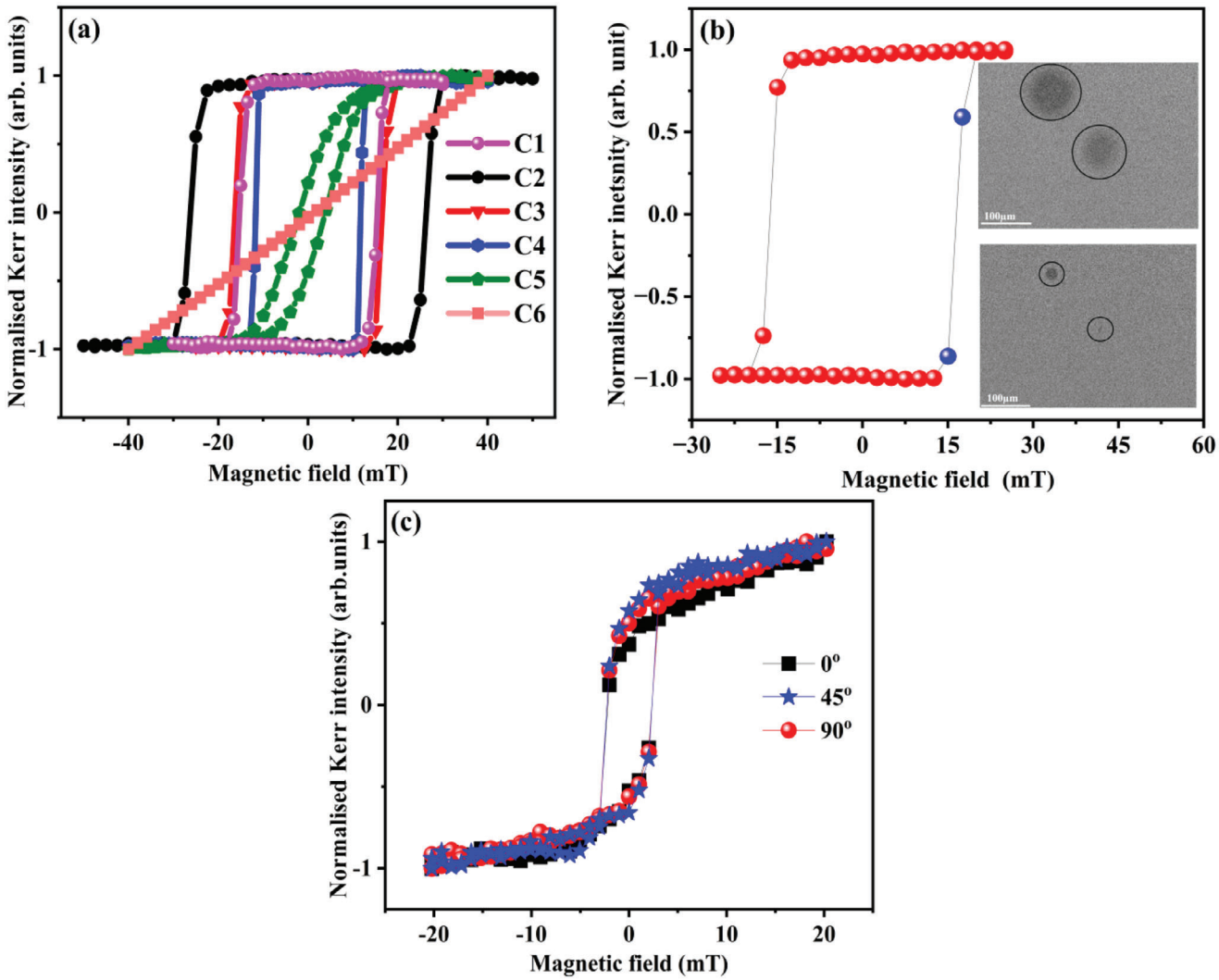

Figure 4. a) PMOKE hysteresis loops for Ta (4 nm)/Pd (4 nm)/Co (t_{Co} nm)/Pd (2 nm) for different thicknesses of the Co layer; b) Bubble domain (inside black circles) nucleation corresponding to magnetic field values shown in blue symbols observed using Kerr microscopy in C3- Ta (4 nm)/Pd (4 nm)/Co (0.6 nm)/Pd (2 nm) during magnetization reversal; c) LMOKE hysteresis for sample C6 – Ta (4 nm)/Pd (4 nm)/Co (1.5 nm)/Pd (2 nm).

$\ln(v_0)$ as a function of t_{Co} also shows linear variation as depicted in Figure 5d.

The damping parameter and the MPE have a strong impact on the spin transport properties across the interfaces of the HM/FM heterostructures. The interdiffusion of HM and FM atoms across the interfaces felicitates the 3d-5d hybridizations which in turn contributes to the MPE. The MPE in HM was found to influence the damping parameter also.[46]

Figure 6 shows the Kerr microscopy image of magnetic bubble domains in C1, C3 and C4 samples, respectively captured under an applied out -of-plane field of 12.8 mT. In comparison, one can observe that the sample C1 has a large number of nucleation centers with small bubble domains compared to the samples C3 and C4. An enhancement in local defects and structural irregularities induced through interdiffusion of atoms at interfaces can act as pinning centers for DWs by reducing the nucleation field.[57,58] This could be the reason why sample C1, which is having very low Co layer thickness and comparatively large interfacial roughness, has a large number of nucleation sites with small DW motion (Figure 5a) and DW size (Figure 6). From the DW images shown in Figure 6 it is clear that sample C1 with the least Co layer thickness is having smooth DWs whereas it becomes rougher as the thickness of the Co layer increases. The variation in DW roughness can be attributed to the interaction between magnetostatic energy and DW energy.[59,60] The magnetostatic energy will try to increase the DW length (total circumference of the domain), leading to a rougher domain. Since the DW energy (energy required to form domains) is proportional to the DW length, the system will try to reduce the DW energy by preferring a smooth DW by shortening the DW length. Furthermore, the magnetostatic energy is proportional to the square of saturation magnetization (M_s^2) while the DW energy is proportional to the uniaxial magnetic anisotropy (DW energy $\propto K_{uni}^{1/2}$).

We have analyzed the saturation magnetization M_S, anisotropy field H_K, effective anisotropy constant ($K_{eff} = \frac{M_S H_K}{2}$) and the DW

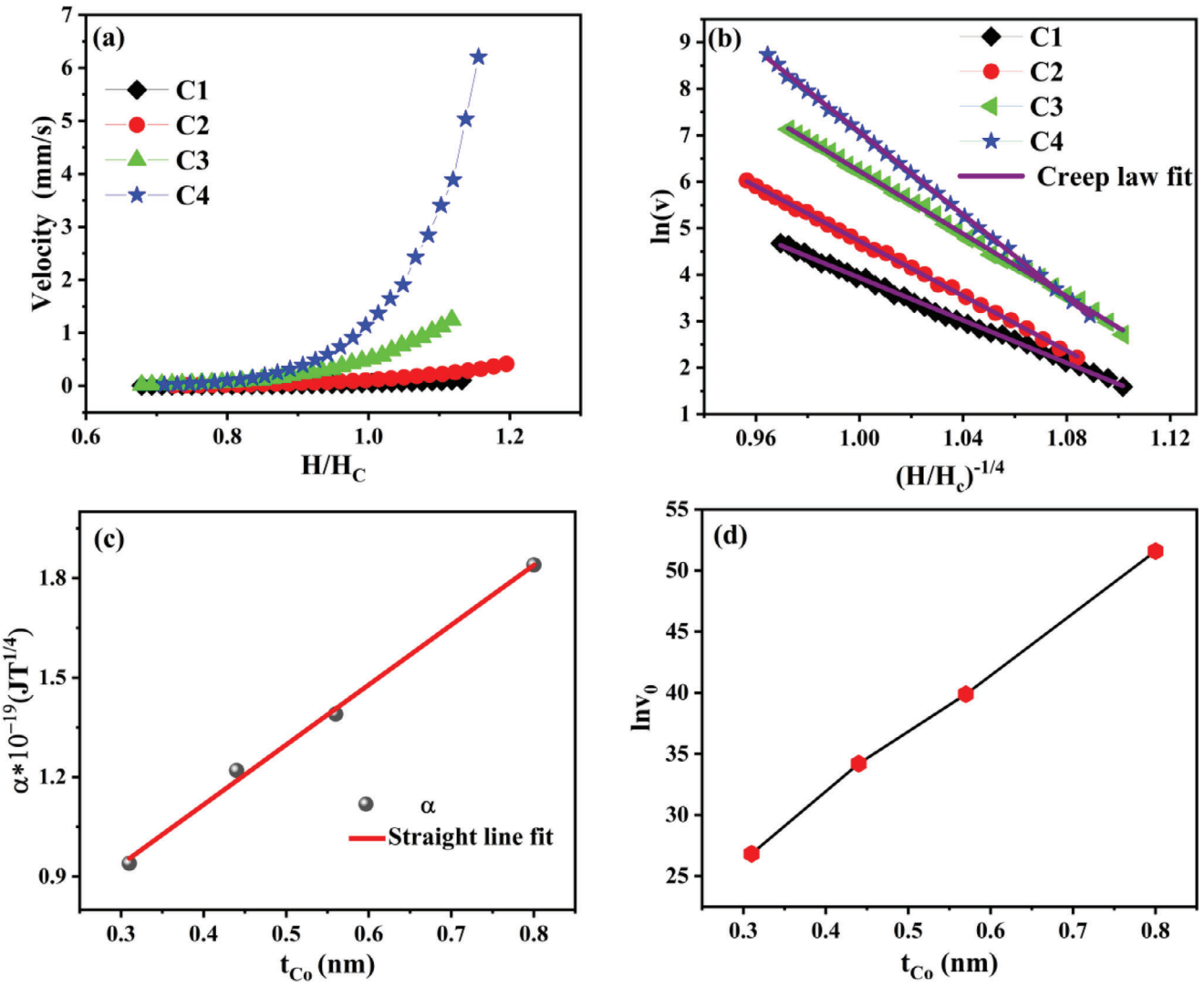

Figure 5. a) Variation of DW velocity as a function of applied magnetic field normalized to the coercivity of each sample. b) Variation of $\ln(v) - (\frac{H}{H_C})^{-1/4}$. c) Variation of α with Co layer thickness values (t_{Co}). d) Variation of $\ln(v_0)$ with t_{Co}. Error bars are within the symbol size.

width $\lambda = \sqrt{\frac{A}{K_{eff}}}$ with exchange stiffness[61] A = 16 $\frac{pJ}{m}$ for Co for the samples C1, C3 and C4 using the VSM results (**Table 2**). The bulk magnetization for the Co layer was noted as 1400 emu/cm^3 from the literature.[62] An increased magnetization compared to the bulk Co value observed here (Table 2) can be attributed to the induced magnetic moment in the Pd layer as a result of the MPE as already evidenced by the MCD-HAXPES at Pd $d_{5/2}$ and XRMR at Pd L_3 edge. The VSM analysis shows that the anisotropy constant K_{eff} decreases with increasing t_{Co}, confirming the FM

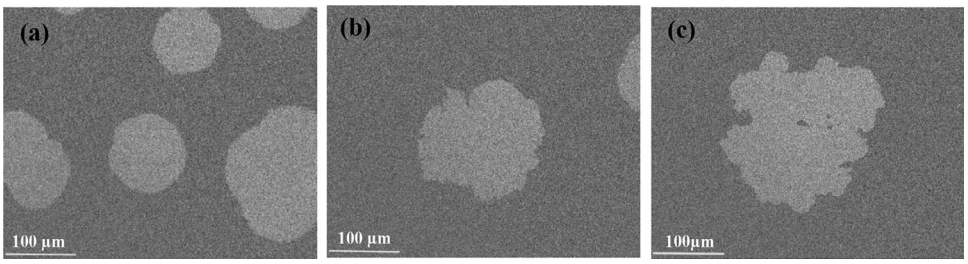

Figure 6. DW images for sample a) C1 b) C3 c) C4, respectively, collected using Kerr microscopy while FIDWM. All images shown are captured at an applied magnetic field of 12.8 mT.

Table 2. Saturation magnetization (M_s), anisotropy filed (H_k) from VSM and calculated anisotropy constant (K_{eff}) and domain wall width (λ) for samples C1, C3 and C4 multilayers in which domain wall dynamics were studied.

Sample	M_s [emu cm^{-3}]	H_k [mT]	K_{eff} [MJ m^{-3}]	λ [nm]
C1	1526 ± 46	1475 ± 10	1.12 ± 0.03	3.78 ± 0.08
C3	1638 ± 18	738 ± 10	0.60 ± 0.02	5.16 ± 0.04
C4	1745 ± 20	533 ± 10	0.47 ± 0.03	5.83 ± 0.09

layer dependent spin reorientation transitions (change in PMA) whereas the DW width increases with increasing t_{Co} (shown in **Figure 7**). Thus, in sample C1 with lower $t_{Co,}$ the DW energy will dominate (high K_{eff}) leading to a smooth domain. As t_{Co} increases, M_s also increases leading to enhanced contribution of magnetostatic energy hence the DW becomes rougher.[56]

In conclusion, the magnetization dynamics in Ta/Pd/Co/Pd system is studied in this work. The thickness values of the FM layer play a crucial role in magnetization dynamics of Pd/Co/Pd multilayers. In the present system, an increase in Co layer thickness leads to spin reorientation transition from out-of-plane to in-plane direction. The FIDWM followed by creep analysis shows enhancement in DW velocity which is in good agreement with the creep scaling law. The systematic increment in DW velocity can be attributed to the decrease of the damping constant with FM layer thickness. The creep scaling constant is correlated with the Co layer thickness and ln(v) shows a linear dependence. Further, the DWs become rough with the increase of the FM layer content due to an increase in magnetostatic energy and decrease of K_{eff} as observed from VSM measurements. Moreover, electronic studies using HAXPES reveals the presence of CoPd alloying at the interfaces. XAFS performed in out-of-plane and in-plane geometry shows the disordered nature of Co with an interdiffusion of Pd atoms into Co layer causing a in plane compressive stress in Co and inducing an asymmetry in bonds. The asymmetry in MCD- HAXPES at Pd 3d edge pictures the induced moment in Pd which is consistent with the saturation magnetic moment obtained from VSM and the additional XRMR results. These results give a combined picture of interfaces and interfacial magnetic properties including the domain wall dynamics in Pd/Co/Pd based all metallic heterostructure with FM thickness; which would be helpful in developing HM/FM heterostructures with tailored properties for DW based spintronics devices.

3. Experimental Section

Thin Film Multilayer Growth: Ta (4 nm)/Pd (4 nm)/Co (t_{Co})/Pd (2 nm), with t_{Co} = 0.3, 0.4, 0.6, 0.8, 0.9, and 1.5 nm named as C1, C2, C3, C4, C5, and C6 respectively were deposited on Si(001) substrates at room temperature using dc magnetron sputtering (Orion-8, AJA Int. Inc,). Depositions were carried out at a working pressure value of 3.7 × 10^{-3} mbar with 50 sccm Ar gas flow at a base pressure lower than 6.6 × 10^{-8} mbar. The substrates were rotated at a speed of 20 rpm for uniform deposition of the films. The deposition rate of Ta, Pd and Co layers were maintained at 1.8, 1.5, and 0.72 nm min^{-1}, respectively.

Structural and Electronic Studies: Structural characterization of all as-deposited multilayer films were done using X-ray reflectivity (XRR) (Malvern Panalytical – Empyrean) with Cu-Kα radiation, wavelength λ = 1.5406 Å. XRR data has been fitted using Parratt's formalism.[63]

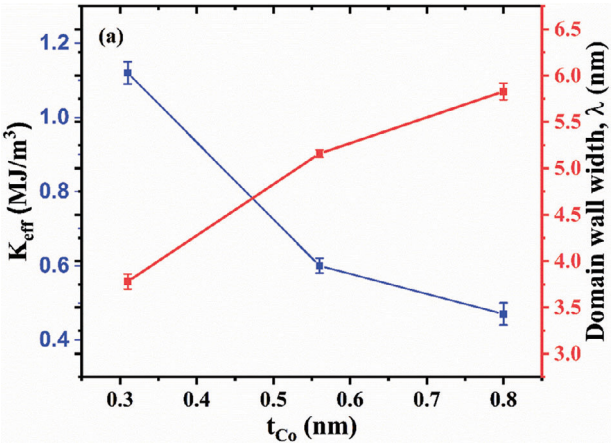

Figure 7. Variation of K_{eff} (blue curve) and calculated domain wall width λ (red curve) with Co layer thickness value t_{Co}.

HAXPES and MCD-HAXPES measurements were performed at beamline P22 of PETRA-III, DESY (Hamburg).[64] The photon energy was set to 6 keV using a Si(311) high heat load double-crystal monochromator. A retractable Fe–Nd–B permanent magnet was used to remanently magnetize the samples in situ along the direction of the photon beam. It supplies an induction field of about 1T, which is high enough to saturate the magnetization of the thin films. MCD was measured at fixed magnetization by changing the helicity of the photons.

Extended X-ray Absorption Fine Structure (EXAFS) spectra were collected at the Co K-edge at the I18 beamline at Diamond Light Source (UK).[65] The samples were mounted using two different geometries, so that the polarization vector of the incoming radiation was parallel or perpendicular to the film plane. The different orientations of the polarization vector correspond to different sensitivities of the XANES data in the film plane or perpendicular to it. The comparison of the data collected in the two geometries provides a reliable assessment of the film average structure in the two directions.[66] The beam size was chosen so to have the full beam footprint within the sample surface. To increase the signal to noise ratio, several scans were repeated keeping the samples under the same experimental conditions. The spectra were averaged and then treated using the standard procedures for XANES analysis[67] using the Athena software.[68]

Magnetic Measurements: Magnetic characterization was performed using a Kerr microscopy, (M/S Evico Magnetics, Germany) based on MOKE having a white LED source and vibrating sample magnetometry (VSM) (Quantum design). MOKE measurements were performed in two geometries – polar (PMOKE) and longitudinal (LMOKE) to identify the magnetic easy axis of each film. To study the DW dynamics, FIDWM was employed using the same Kerr microscopy system with an additional power supply (Kepco power supply) to produce pulsed magnetic fields.[19] Differential subtraction is employed here in which initially the samples are saturated with maximum magnetic field and the image is captured as background then the background is subtracted from subsequent Kerr microscopy images to obtain the domain images. Domain wall velocity calculations were done using a suitable algorithm developed in python environment by Raj et al.[19,69] Super conducting quantum interference device (SQUID) – VSM (Quantum Design) was performed at room temperature to obtain the effective magnetic moment, anisotropy constant and the DW width.

Supporting Information

Supporting Information is available from the Wiley Online Library or from the author.

Acknowledgements

A.K. and S.K.V. acknowledge UGC DAE-CSR Indore for providing financial support under the collaborative research scheme (CRS/2021-22/01/353). We acknowledge DESY (Hamburg, Germany), a member of the Helmholtz Association HGF, for the provision of experimental facilities. Parts of this research were carried out at beamlines P09 and P22 at DESY and the authors would like to thank Dr. Sonia Francoual, P09 beamline, for her support in performing the XRMR measurements. XRMR and HAXPES beamtimes were allocated for proposals II-20211057 and I-20221079, respectively. Financial support by Department of Science and Technology (DST), Government of India within the frame work of the India-DESY collaboration to conduct experiments at PETRA III DESY is highly acknowledged. The support of Dr. Konstantin Igniatyev during the EXAFS data collection at the I18 beamline is also acknowledged. The authors acknowledge Er. Layanta Behera and Er. Anil Gome, UGC-DAE CSR, Indore, India, for helping with thin film deposition using sputtering technique and XRR measurements, respectively. The authors acknowledge Dr. Ram Janay Chowdhary, UGC-DAE CSR, Indore, India, for SQUID-VSM measurements. Central Instrumentation Centre (CIC) of R&D UPES, Dehradun for XRR measurements is acknowledged.

Open access funding enabled and organized by Projekt DEAL.

Conflict of Interest

The authors declare no conflict of interest.

Data Availability Statement

The data that support the findings of this study are available in the supplementary material of this article.

Keywords

interdiffusion, magnetic domain wall velocity, magnetic thin films, magneto optical Kerr microscopy, perpendicular magnetic anisotropy

Received: October 9, 2024
Revised: January 2, 2025
Published online: February 5, 2025

[1] A. Soumyanarayanan, N. Reyren, A. Fert, C. Panagopoulos, *Nature* **2016**, *539*, 509.
[2] A. Fert, V. Cros, J. Sampaio, *Nat. Nanotechnol.* **2013**, *8*, 152.
[3] S. D. Pollard, J. A. Garlow, J. Yu, Z. Wang, Y. Zhu, H. Yang, *Nat. Commun.* **2017**, *8*, 14761.
[4] J. Brandão, D. A. Dugato, R. L. Seeger, J. C. Denardin, T. J. A. Mori, J. C. Cezar, *Sci. Rep.* **2019**, *9*, 4144.
[5] P. F. Carcia, *J. Appl. Phys.* **1988**, *63*, 5066.
[6] S. Kayal, S. Maji, A. Mukhopadhyay, P. S. Anil Kumar, *J. Magn. Magn. Mater.* **2022**, *558*, 169499.
[7] W. Zhang, M. B. Jungfleisch, W. Jiang, Y. Liu, J. E. Pearson, S. G. E. T. Velthuis, A. Hoffmann, F. Freimuth, Y. Mokrousov, *Phys. Rev. B* **2015**, *91*, 115316.
[8] I. Dzyaloshinsky, *J. Phys. Chem. Solids* **1958**, *4*, 241.
[9] T. Moriya, *Phys. Rev.* **1960**, *120*, 91.
[10] A. W. J. Wells, P. M. Shepley, C. H. Marrows, T. A. Moore, *Phys. Rev. B* **2017**, *95*, 054428.
[11] A. V. Davydenko, A. G. Kozlov, M. E. Stebliy, A. G. Kolesnikov, N. I. Sarnavskiy, I. G. Iliushin, A. P. Golikov, *Phys. Rev. B* **2021**, *103*, 094435.
[12] M. S. N. Tey, X. Chen, A. Soumyanarayanan, P. Ho, *ACS Appl. Electron. Mater.* **2022**, *4*, 5088.
[13] A. Fert, N. Reyren, V. Cros, *Nat. Rev. Mater.* **2017**, *2*, 17031.
[14] S. Peng, D. Zhu, W. Li, H. Wu, A. J. Grutter, D. A. Gilbert, J. Lu, D. Xiong, W. Cai, P. Shafer, K. L. Wang, W. Zhao, *Nat. Electron.* **2020**, *3*, 757.
[15] W. Li, Z. Liu, S. Peng, J. Lu, J. Liu, X. Li, S. Lu, Y. Otani, W. Zhao, *IEEE Electron Device Lett.* **2024**, *45*, 921.
[16] R. Wang, Z. Xiao, H. Liu, Z. Quan, X. Zhang, M. Wang, M. Wu, X. Xu, *Appl. Phys. Lett.* **2019**, *114*, 042404.
[17] K.-S. Ryu, L. Thomas, S.-H. Yang, S. Parkin, *Nat. Nanotechnol.* **2013**, *8*, 527.
[18] H. Yang, A. Thiaville, S. Rohart, A. Fert, M. Chshiev, *Phys. Rev. Lett.* **2015**, *115*, 267210.
[19] R. Raj, Z. Hussain, D. Kumar, V. R. Reddy, *Meas. Sci. Technol.* **2023**, *34*, 097001.
[20] S. K. V, D. Kumar, V. Ganesan, A. Gupta, *Appl. Surf. Sci.* **2012**, *258*, 4116.
[21] A. Mukhopadhyay, S. Maji, P. S. Anil Kumar, *J. Magn. Magn. Mater.* **2021**, *537*, 168125.
[22] I. Vaskivskyi, R. S. Malik, L. Salemi, D. Turenne, R. Knut, J. Brock, R. Stefanuik, J. Söderström, K. Carva, E. E. Fullerton, P. M. Oppeneer, O. Karis, H. A. Dürr, *J. Phys. Chem. C* **2021**, *125*, 11714.
[23] A. Mukhopadhyay, S. Koyiloth Vayalil, D. Graulich, I. Ahamed, S. Francoual, A. Kashyap, T. Kuschel, P. S. Anil Kumar, *Phys. Rev. B* **2020**, *102*, 144435.
[24] D.-O. Kim, K. M. Song, Y. Choi, B.-C. Min, J.-S. Kim, J. W. Choi, D. R. Lee, *Sci. Rep.* **2016**, *6*, 25391.
[25] R. M. Rowan-Robinson, A. A. Stashkevich, Y. Roussigné, M. Belmeguenai, S.-M. Chérif, A. Thiaville, T. P. A. Hase, A. T. Hindmarch, D. Atkinson, *Sci. Rep.* **2017**, *7*, 16835.
[26] V. M. Parakkat, K. R. Ganesh, P. S. Anil Kumar, *AIP Adv.* **2016**, *6*, 056122.
[27] J. Cho, N.-H. Kim, S. Lee, J.-S. Kim, R. Lavrijsen, A. Solignac, Y. Yin, D.-S. Han, N. J. J. Van Hoof, H. J. M. Swagten, B. Koopmans, C.-Y. You, *Nat. Commun.* **2015**, *6*, 7635.
[28] X. Zhao, B. Zhang, N. Vernier, X. Zhang, M. Sall, T. Xing, L. H. Diez, C. Hepburn, L. Wang, G. Durin, A. Casiraghi, M. Belmeguenai, Y. Roussigné, A. Stashkevich, S. M. Chérif, J. Langer, B. Ocker, S. Jaiswal, G. Jakob, M. Kläui, W. Zhao, D. Ravelosona, *Appl. Phys. Lett.* **2019**, *115*, 122404.
[29] J. T. Kohlhepp, G. J. Strijkers, H. Wieldraaijer, W. J. M. De Jonge, *Phys. Status Solidi A* **2002**, *189*, 701.
[30] J. Carrey, A. E. Berkowitz, W. F. Egelhoff, D. J. Smith, *Appl. Phys. Lett.* **2003**, *83*, 5259.
[31] S.-K. Kim, Y.-M. Koo, V. A. Chernov, J. B. Kortright, S.-C. Shin, *Phys. Rev. B.* **2000**, *62*, 3025
[32] J. Vogel, M. Bonfim, N. Rougemaille, O. Boulle, I. M. Miron, S. Auffret, B. Rodmacq, G. Gaudin, J. C. Cezar, F. Sirotti, S. Pizzini, *Phys. Rev. Lett.* **2012**, *108*, 247202.
[33] C. A. F. Vaz, D. Prabhakaran, E. I. Altman, V. E. Henrich, *Phys. Rev. B* **2009**, *80*, 155457.
[34] P. Vishwakarma, M. Nayak, V. R. Reddy, A. Gloskovskii, W. Drube, A. Gupta, *Appl. Surf. Sci.* **2022**, *590*, 153063.
[35] U. Bardi, *J. Catal.* **1990**, *124*, 22.
[36] G. Martinez, A. Malumbres, A. Lopez, R. Mallada, J. L. Hueso, J. Santamaria, *Front. Chem.* **2018**, *6*, 487.
[37] M. C. Biesinger, B. P. Payne, A. P. Grosvenor, L. W. M. Lau, A. R. Gerson, R. St. C. Smart, *Appl. Surf. Sci.* **2011**, *257*, 2717.
[38] A. P. Grosvenor, S. D. Wik, R. G. Cavell, A. Mar, *Inorg. Chem.* **2005**, *44*, 8988.
[39] G. H. Fecher, D. Ebke, S. Ouardi, S. Agrestini, C.-Y. Kuo, N. Hollmann, Z. Hu, A. Gloskovskii, F. Yakhou, N. B. Brookes, C. Felser, *SPIN* **2014**, *04*, 1440017.

[40] G. Panaccione, G. Van Der Laan, H. A. Dürr, J. Vogel, N. B. Brookes, *Eur. Phys. J. B* **2001**, *19*, 281.
[41] T. Kuschel, C. Klewe, J.-M. Schmalhorst, F. Bertram, O. Kuschel, T. Schemme, J. Wollschläger, S. Francoual, J. Strempfer, A. Gupta, M. Meinert, G. Götz, D. Meier, G. Reiss, *Phys. Rev. Lett.* **2015**, *115*, 097401.
[42] S. Macke, E. Goering, *J. Phys.: Condens. Matter* **2014**, *26*, 363201.
[43] I. Carlomagno, J. Drnec, A. M. Scaparro, S. Cicia, S. Vlaic, R. Felici, C. Meneghini, *J. Appl. Phys.* **2016**, *120*, 195302.
[44] J. Miyawaki, D. Matsumura, A. Nojima, T. Yokoyama, T. Ohta, *Surf. Sci.* **2007**, *601*, 95.
[45] P. C. Carvalho, I. P. Miranda, J. Brandão, A. Bergman, J. C. Cezar, A. B. Klautau, H. M. Petrilli, *Nano Lett.* **2023**, *23*, 4854.
[46] C. Swindells, H. Głowiński, Y. Choi, D. Haskel, P. P. Michałowski, T. Hase, P. Kuświk, D. Atkinson, *Appl. Phys. Lett.* **2021**, *119*, 152401.
[47] J. Okabayashi, Y. Miura, H. Munekata, *Sci. Rep.* **2018**, *8*, 8303.
[48] J. Dho, *IEEE Trans. Magn.* **2022**, *58*, 9901147.
[49] S. Eimer, H. Cheng, J. Li, X. Zhang, C. Zhao, W. Zhao, *Sci. China Inf. Sci.* **2023**, *66*, 122408.
[50] B. Rakesh, N. Bhagat, D. Gupta, B. Pandey, *J. Mater. Sci.: Mater. Electron.* **2024**, *35*, 1271.
[51] P. J. Metaxas, J. P. Jamet, A. Mougin, M. Cormier, J. Ferré, V. Baltz, B. Rodmacq, B. Dieny, R. L. Stamps, *Phys. Rev. Lett.* **2007**, *99*, 217208.
[52] E. Jué, C. K. Safeer, M. Drouard, A. Lopez, P. Balint, L. Buda-Prejbeanu, O. Boulle, S. Auffret, A. Schuhl, A. Manchon, I. M. Miron, G. Gaudin, *Nat. Mater.* **2016**, *15*, 272.
[53] E. Barati, M. Cinal, D. M. Edwards, A. Umerski, *EPJ Web Conf.* **2013**, *40*, 18003.
[54] S. Mizukami, E. P. Sajitha, D. Watanabe, F. Wu, T. Miyazaki, H. Naganuma, M. Oogane, Y. Ando, *Appl. Phys. Lett.* **2010**, *96*, 152502.
[55] C. P. Quinteros, S. Bustingorry, J. Curiale, M. Granada, *Appl. Phys. Lett.* **2018**, *112*, 262402.
[56] D.-Y. Kim, M.-H. Park, Y.-K. Park, J.-S. Yu, J.-S. Kim, D.-H. Kim, B.-C. Min, S.-B. Choe, *Appl. Phys. Lett.* **2018**, *112*, 062406.
[57] A. Aharoni, *Rev. Mod. Phys.* **1962**, *34*, 227.
[58] A. Aharoni, *J. Appl. Phys.* **1961**, *32*, S245.
[59] K.-W. Moon, D.-H. Kim, S.-C. Yoo, C.-G. Cho, S. Hwang, B. Kahng, B.-C. Min, K.-H. Shin, S.-B. Choe, *Phys. Rev. Lett.* **2013**, *110*, 107203.
[60] S. Lemerle, J. Ferré, C. Chappert, V. Mathet, T. Giamarchi, P. L. Doussal, *Phys. Rev. Lett.* **1998**, *80*, 849.
[61] C. Eyrich, W. Huttema, M. Arora, E. Montoya, F. Rashidi, C. Burrowes, B. Kardasz, E. Girt, B. Heinrich, O. N. Mryasov, M. From, O. Karis, *J. Appl. Phys.* **2012**, *111*, 07C919.
[62] R. I. Allen, F. W. Constant, *Phys. Rev.* **1933**, *44*, 228.
[63] L. G. Parratt, *Phys. Rev.* **1954**, *95*, 359.
[64] C. Schlueter, A. Gloskovskii, K. Ederer, I. Schostak, S. Piec, I. Sarkar, Y. Matveyev, P. Lömker, M. Sing, R. Claessen, C. Wiemann, C. M. Schneider, K. Medjanik, G. Schönhense, P. Amann, A. Nilsson, W. Drube, *AIP Conf. Proc.* **2019**, *2054*, 040010.
[65] J. F. W. Mosselmans, P. D. Quinn, A. J. Dent, S. A. Cavill, S. D. Moreno, A. Peach, P. J. Leicester, S. J. Keylock, S. R. Gregory, K. D. Atkinson, J. R. Rosell, *J Synchrotron Radiat.* **2009**, *16*, 818.
[66] I. Carlomagno, J. Drnec, A. M. Scaparro, S. Cicia, S. Mobilio, R. Felici, C. Meneghini, *Chem. Phys. Lett.* **2018**, *697*, 7.
[67] G. Bunker, *Introduction to XAFS: A Practical Guide to X-Ray Absorption Fine Structure Spectroscopy*, Cambridge University Press, Cambridge, **2010**.
[68] B. Ravel, M. Newville, *J. Synchrotron Radiat.* **2005**, *12*, 537.
[69] R. Raj, V. R. Reddy, *Meas. Sci. Technol.* **2025**, *36*, 017005.